NJC

PAPER

Cite this: *New J. Chem.*, 2015, **39**, 3929

The synthesis of an octasubstituted monohydroxylated phthalocyanine designed to investigate the effect of the presence of active moieties†

Deniz Kutlu Tarakci,[ab] Savaş Berber,[c] Yunus Zorlu,[a] Devrim Atilla,[a] Vefa Ahsen[a] and Fabienne Dumoulin*[a]

Received (in Montpellier, France) 27th January 2015,
Accepted 5th March 2015

DOI: 10.1039/c5nj00229j

www.rsc.org/njc

A monohydroxylated octasubstituted phthalocyanine, aimed at being used as a synthon for further conjugation, has been designed to offer rigorous comparison conditions to study the effect of the presence of an active moiety, compared to its non-functionalized symmetric analogs. After the validation of the concept using computational methods, the designed phthalocyanine was prepared and exhibited the expected suitable electronic absorption properties. Biotin conjugation was performed.

Introduction

The substitution pattern of phthalocyanines has crucial effects on its properties, and can in particular strongly affect its spectroscopic properties, as we recently demonstrated in a fundamental study investigating the modulation of the spectroscopic and electronic properties of octasubstituted Zn(II) phthalocyanines.[1] The number of substituents is another factor, and octasubstituted phthalocyanines exhibit a Q band which is red-shifted compared to the corresponding tetra-substituted derivative.[2] All else being equal, the difference in the maximum absorption of tetra- or octasubstituted phthalocyanines reaches up to 20 nm.[3] A difference of 7 nm in the maximum absorption of octa- and heptaalkylsulfanyl substituted Zn(II) phthalocyanines has been observed.[4] The fluorescence properties are similarly affected by the number of substituents.[5]

Monofunctionalization of phthalocyanines is of particular importance in the preparation of materials. Grafting active moieties onto phthalocyanines allows us to combine two properties and to obtain dual effects for biomedical applications. The photosensitizing ability of phthalocyanines used in photodynamic therapy has been combined with the imaging properties of Gd-DOTA,[6] to the antivascular effect of chalcones,[7] to the tumour targeting effect of antibodies[8] or several active moieties such as carbohydrates,[9] folic acid.[10] Phthalocyanines can be functionalized for other purposes as well: grafting onto polymers[11] and nanoparticles,[12] and conjugation with energy-transfer or electron-transfer units, among others.

In most of the cases, the functionalization is introduced by the preparation of A3B-type phthalocyanines, by the statistical cyclotetramerisation of the phthalonitrile B carrying the function (possibly modified again after the formation of the macrocycle), and phthalonitrile A substituted suitably to provide the desired solubility. The A4 symmetrically substituted derivative is commonly used as the reference compound to investigate the effect of the presence of the functionalization and of the active moiety, as illustrated on Fig. 1A. In all cases of functionalization, it is useful to know if the introduction of the unit has an effect on the spectroscopic properties of the phthalocyanines. Nevertheless, rigorous comparison conditions may not be met, depending on the similarity of substituents of phthalonitriles A and B, likely to prevent a comparison *ceteris paribus*.

Results and discussion

Molecular design

Aiming at proposing structures functionalized for the rigorous evaluation of the effect of the presence of active moieties on phthalocyanine properties, we listed the required structural features to gather in order to elaborate a suitable molecular design:

– to work on octasubstituted derivatives, to avoid the effect of isomeric mixtures.

– to have the same atoms linking the substituents of the four isoindole subunits of functionalized Pc and on the reference Pc to have a similar electronic configuration on the phthalocyanine ring,

– to have similar solubility and aggregation state.

[a] *Gebze Technical University, Department of Chemistry, P. O. Box 141 Gebze, 41400 Kocaeli, Turkey. E-mail: fdumoulin@gyte.edu.tr; Fax: +90 262 605 30 05; Tel: +90 262 605 30 22*

[b] *Yildiz Technical University, Faculty of Sciences, Department of Chemistry, 34210 Esenler, Istanbul, Turkey*

[c] *Gebze Technical University, Department of Physics, P. O. Box 141 Gebze, 41400 Kocaeli, Turkey*

† Electronic supplementary information (ESI) available. CCDC 968416 (3). For ESI and crystallographic data in CIF or other electronic format see DOI: 10.1039/c5nj00229j

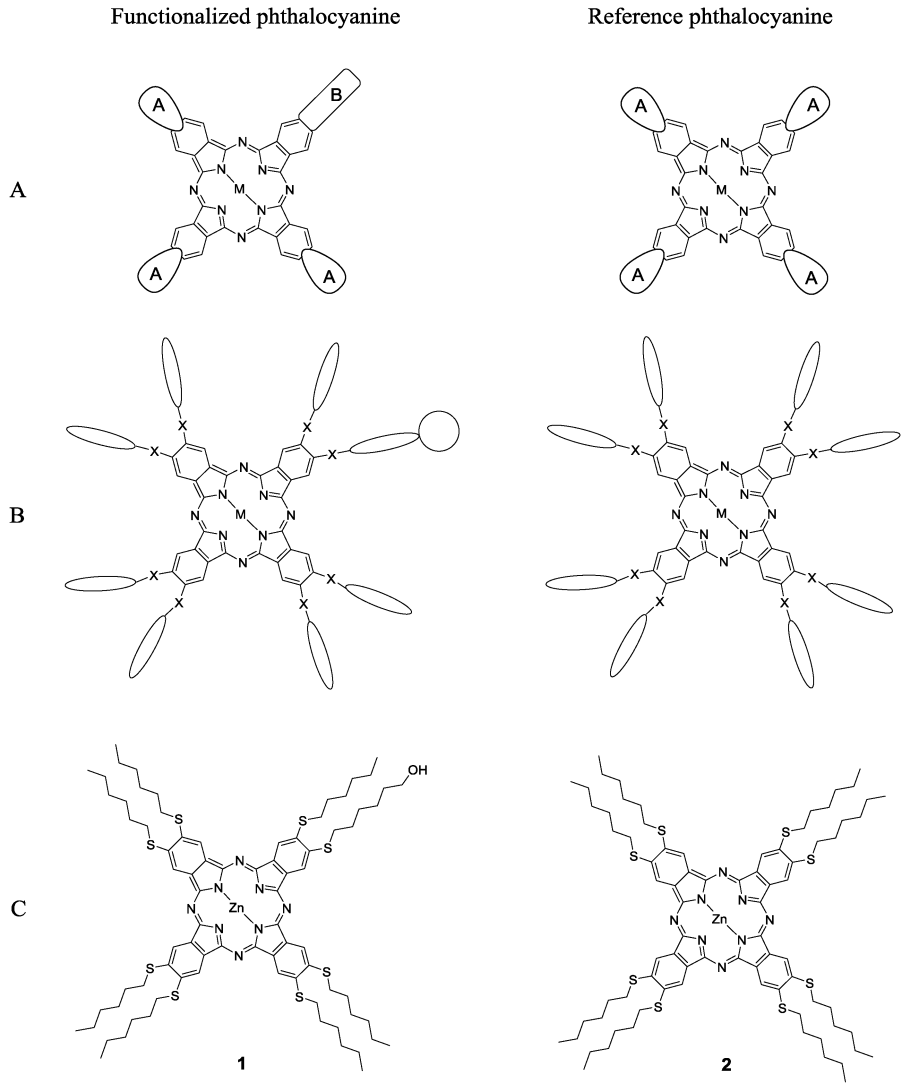

Fig. 1 Molecular design of functionalized phthalocyanine **1** and the related reference derivative **2**.

These considerations are structurally summarized in Fig. 1B.

Alkylsulfanyl substitution offers several advantages, among which an easy synthesis by the direct reaction of thiol on dichlorophthalonitrile, when the preparation of analogous alkoxy derivatives is tedious, implying at least three steps. The commercial availability of hydroxylated thiols is another advantage, and they have been widely used to prepare functionalized phthalocyanines.[13–15] Octahexylsulfanyl phthalocyanines are known to be soluble and non-aggregated in a wide range of solvents. Based on these data, we designed the monohydroxylated octaalkylsulfanyl substituted phthalocyanine **1**, to be compared with the octahexylsulfanyl substituted phthalocyanine **2** (Fig. 1C). Phthalocyanine **1** was aimed at being used as a synthon for further conjugation with active moieties, to study the effect of their presence on the electronic properties of the conjugate comparatively to reference phthalocyanine **2**.

Computational assessment of the concept

We first of all wished to assess the relevance of the molecular design and of the concept developed here using computational methods. The proposed atomic structures were optimized and their electronic structures calculated within the density functional theory. The frontier orbitals of phthalocyanines **1** and **2**, which are depicted as 3D isosurfaces, are compared in Fig. 2, where the energy level for each orbital is given below the corresponding orbital. While the highest occupied molecular orbital (HOMO) level is non-degenerate, the lowest unoccupied molecular orbital (LUMO) levels are degenerate within the numerical accuracy of our calculations. Therefore, both LUMO orbitals are shown in Fig. 2. The energy levels and frontier orbitals are essentially the same for phthalocyanines **1** and **2** with a very small upshift for phthalocyanine **1**. The fundamental energy gap also remains the same after hydroxyl functionalization. Therefore, the frontier molecular orbitals and their energy levels are essentially unaltered by the chemical modification that is far from the core region of the phthalocyanine. Since the energy levels of the side chains are strong σ-states, they lie well below the Fermi level and thus do not influence the frontier orbitals, which are π-states. Therefore, our calculated frontier orbitals with full side chains, displayed

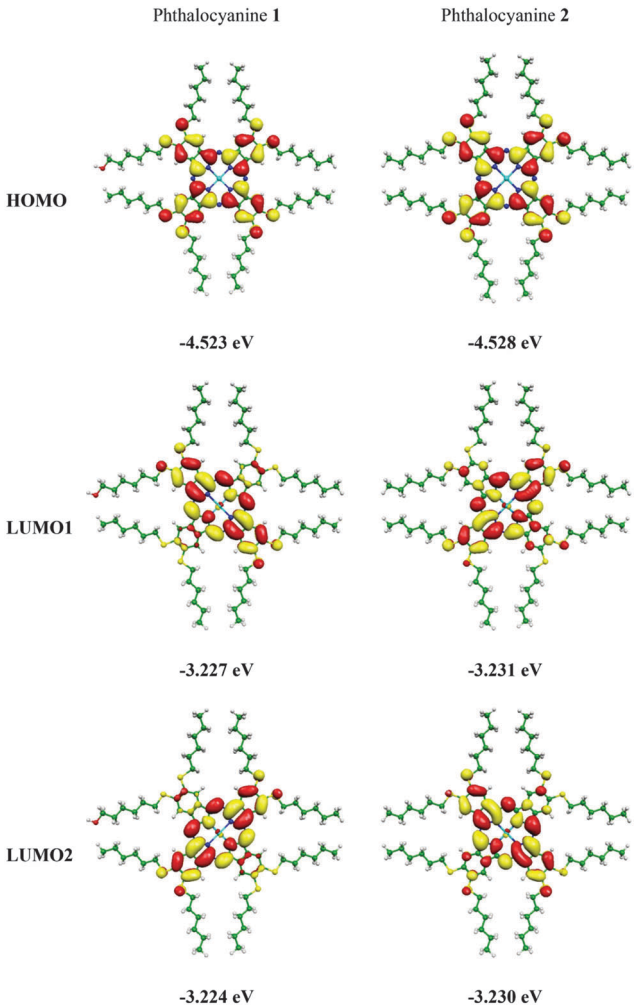

Fig. 2 Frontier orbitals of phthalocyanines **1** and **2** depicted as 3D isosurfaces. Energy level for each orbital is given below the corresponding orbital. Different colors are to distinguish the opposite phases of the wavefunctions.

in Fig. 2, are identical to the results for $-CH_3$ terminated phthalocyanines previously reported by us.[1] Electronic transitions between our calculated frontier orbital energy levels correspond to absorptions at 730 nm, 477 nm, and 412 nm.

In order to investigate the electronic structure of phthalocyanines **1** and **2** in a wider energy range, we calculated the electronic density of states (DOS) for each molecule (Fig. S1, ESI†). The energy levels are given with respect to the Fermi level of each molecule, which is the midpoint between HOMO and LUMO levels. The reduction of the symmetry by the inclusion of a hydroxyl group changes the energy levels by very small values. However, even these very small splitting of energy levels decreases the peak values of the DOS, which are originated from the degenerate states. The splitting of levels into very close energy levels result in a broadening of the DOS. Thus, the peaks in the electronic spectra are expected to appear at the same wavelength values while only a small reduction of the intensities are possible due to the reduced DOS values for phthalocyanine **1**.

Having confirmed the relevance of the concept, the designed molecules have been synthesized.

Synthesis

A3B phthalocyanines are easily prepared by cyclotetramerisation of a statistical mixture of two phthalonitriles respectively of A and B type. In this work, B-type phthalonitrile is the compound **3**, newly reported here, whereas A-type phthalonitrile is compound **4**. To obtain concomitantly phthalonitriles **3** and **4**, 4,5-dichlorophtalonitrile was reacted with a mixture of hexanethiol and 6-mercaptohexanol (Scheme 1). After several attempts, the best yield in **3** was obtained for a 1 : 1 : 1 mixture of these three reactants.

Suitable crystals for X-ray diffraction study of the precursor **3** were grown *via* recrystallization from ethanol. The ORTEP representation of molecular structure with atomic numbering scheme is shown in Fig. 3a. Compound **3** crystallizes in a triclinic space group ($P\bar{1}$). The bond lengths and angles are all in normal values. Both (hydroxyhexyl)thio and hexylthio moieties are nearly planar to the phenyl ring (C3–C8). In the crystal structure, the intermolecular O–H···N [O1···N2 = 2.980(3) Å] hydrogen bonding interactions link adjacent molecules to give $R(30)_2^2$ motif (Fig. 3b).

Phthalocyanines **1** and **2** were obtained by a statistical mixed condensation of phthalonitriles **3** and **4**, and were easily separated chromatographically thanks to their different polarities. Monohydroxylated phthalocyanine **1** was obtained in 13% yield, in accordance with usual yields for such A3B derivatives.[16–19]

Comparative analysis

Due to the aggregation of monohydroxylated phthalocyanine **1** at the concentrations requested to record a NMR spectrum (much higher than for UV-Vis investigations), NMR comparative studies could not be conducted on the NMR spectra of **1** and **2**. Anyway, the electronic similarity of phthalonitriles **3** and **4** has been assessed by superimposition of their NMR spectra (Fig. S2, ESI†), assuming that the electronic similarity of

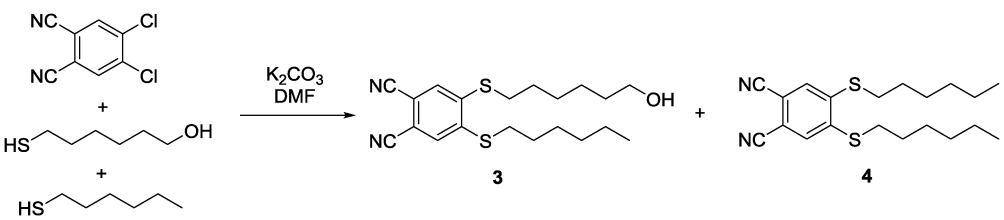

Scheme 1 Preparation of monohydroxylated phthalonitrile **3**.

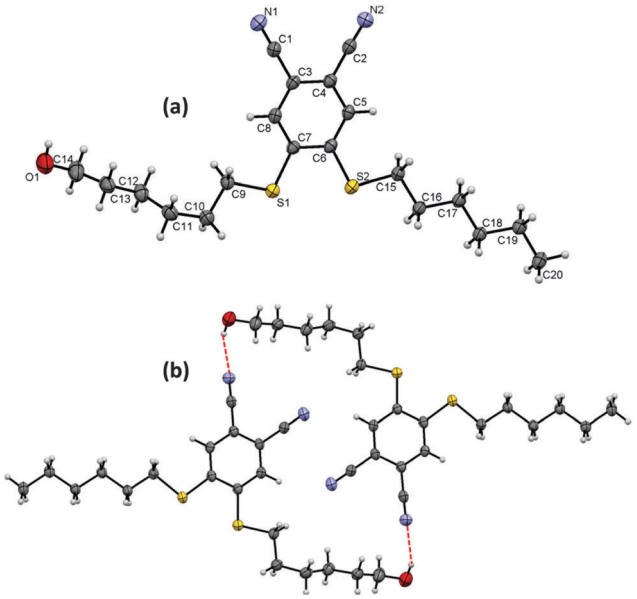

Fig. 3 (a) Structure of phthalonitrile compound **3**. Displacement ellipsoids are drawn at the 50% probability level. H-atoms are shown as small spheres of arbitrary radii (b) hydrogen bonding interactions in compound **3**, showing $R(30)_2^2$ motif. Selected bond lengths (Å): C1–N1 1.151(4); C2–N2 1.143(3); C9–S1 1.812(3); C15–S2 1.813(3); C7–S1 1.753(2); C6–S2 1.747(2). Selected bond angles (°): C7–S1–C9 103.23(12); C6–S2–C15 104.03(12); N1–C1–C3 178.1(3); N2–C2–C4 178.6(3); C5–C6–S2 123.45(19); C8–C7–S1 123.75(19); C7–C6–S2 117.17(18).

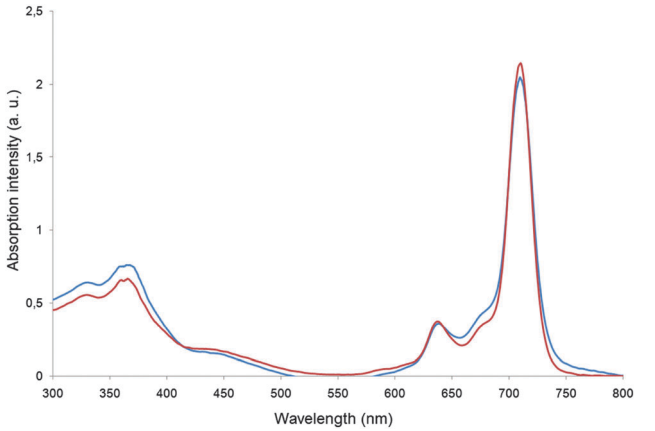

Fig. 4 Superposition of the UV-Vis electronic absorption spectra of phthalocyanines **1** (blue) and **2** (red), evidencing the same maximum of their Q band (10 μM in chloroform).

the phthalonitriles implies the electronic similarity of the corresponding phthalocyanines. The chemical shift of a proton or of a carbon is very specific, and the more similar the two molecules are, the more similar are their NMR spectra. We focused on the aromatic area of the spectra, corresponding to the atoms that will be part of the future phthalocyanine skeleton. **3** and **4** exhibit a same chemical shift at 7.40 ppm for the aromatic protons of each phthalonitrile (Fig. S2a and b, ESI†). Magnification of this area of the spectra (Fig. S2c and d, ESI†) showed that the presence of the hydroxyl induces a differentiation, as evidenced by the very small 2 Hz value of the coupling constant. In ^{13}C NMR spectra (Fig. S3, ESI†), chemical shift of the aromatic carbons are centred exactly at the same values, with a minor differentiation induced by the presence of the hydroxyl group.

Comparative observation of electronic absorption spectra of **1** and **2** (Fig. 4) was actually the best way to evidence the relevance of our molecular design. Recorded in chloroform at identical concentrations, the results follow the computational predictions, with a similar maximum of the Q band at 710 nm and a perfect fit of the different bands maxima. The presence of the hydroxyl on **1** induced only trivial discrepancy between the intensity of the bands observed.

All these observations confirm the relevance of our molecular design, regarding the parameters listed above. The solubility similarity and monomeric non-aggregated state of **1** is evidenced by the sharp shape of its Q band (Fig. 4), and the maximum absorption of **1** and **2** is perfectly superimposable, despite minor intensity variations.

Electronic transitions between our calculated frontier orbital energy levels correspond to the absorption wavelengths that are slightly higher than the peak positions in our measured UV spectrum since density functional theory underestimates energy gaps and lower transition energies translate into higher wavelengths.[20]

Application to biotinylation

Targeting strategies in PDT, our main field of research, follow several directions. Among the conjugation to targeting moieties and as evocated above, folic acid conjugation has already been successfully used on PDT photosensitisers.[21–23] It is based on the overexpression of the folate receptor by cancer cells, due to their elevated metabolic needs. For a similar reason, biotin is now used as an alternative targeting unit for cancer therapies and imaging techniques,[24,25] and at least once photodynamic therapy.[26] This is why we selected biotin as an active moiety to be grafted on phthalocyanine **1**, by the classical DCC/DMAP esterification (Scheme 2), in 79% yield. The structure was unambiguously confirmed by MALDI analysis (Fig. S4, ESI†).

The conjugate **5** proved to be much more polar that phthalocyanine **1**. This induced aggregation of **5** was enhanced by its amphiphilic character (Fig. 5). As a consequence, the intensity of the absorption is lowered, the shape of the Q band is enlarged, and its maximum is blue-shifted by 10 nm. Such a blue shift is characteristic for aggregated species.

Conclusions

In order to optimize the investigation of the effect of the presence of active moieties on photosensitising phthalocyanines, a new substitution pattern has been designed by listing carefully several parameters: octasubstitution, a similar substitution pattern retaining a similar electronic configuration on the phthalocyanine ring for the functionalized and the reference compounds, and similar solubility and aggregation state. After assessment of the relevance of the design by computational

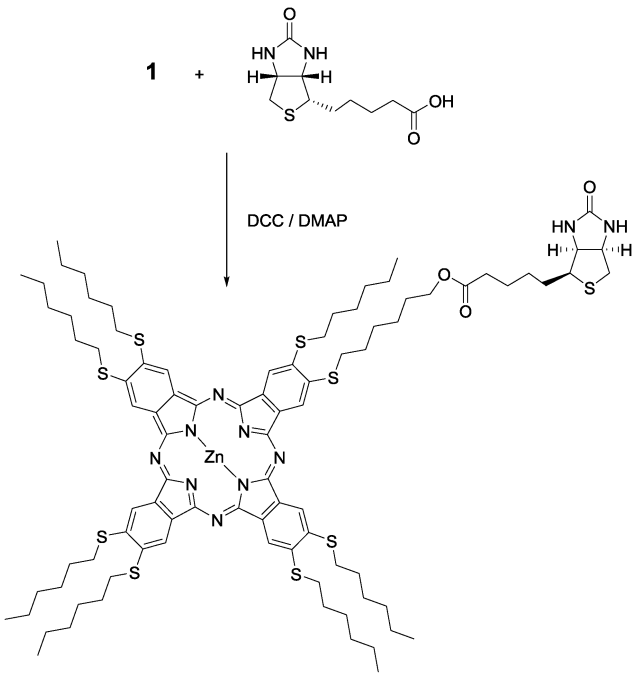

Scheme 2 Preparation of the phthalocyanine–biotin conjugate **5**.

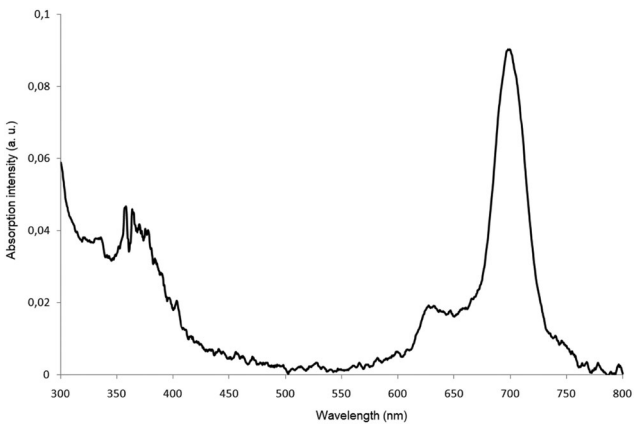

Fig. 5 UV-Vis spectrum of phthalocyanine–biotin conjugate **5** in chloroform (10 μM).

calculations, a monohydroxylated octasubstituted phthalocyanine has been prepared. As expected from the calculations, its UV-Vis absorption spectrum fitted the one of the reference phthalocyanine. A first conjugation with biotin was performed. Its amphiphilicity unfortunately induced a strong aggregation.

Other conjugates with various active moieties of different hydrophilicities are being prepared and further interpretations will be made to establish fully the limits of our concept.

Experimental

Theoretical orbital calculations

Our structure optimization and electronic structure calculations were performed using the SIESTA code[27] in the generalized gradient approximation (GGA) to density functional theory (DFT). The interactions between the core and valence orbitals are taken into account by norm-conserving Troullier–Martins pseudopotentials[28] with partial core corrections in the Kleinman–Bylander fully separable form.[29] The Perdew–Burke–Ernzerhof[30] parameterization is used for the exchange–correlation functional, and a double-ζ basis set augmented by polarization orbitals is used. A real space grid that corresponds to a plane wave cut-off energy of 200 Ry is employed. Before the density of states calculations, the atomic positions are determined by the structure optimizations that are performed in a conjugate-gradient algorithm until all force components on each atom are less than 0.01 eV $Å^{-1}$. The wavefunctions for the fully relaxed molecules are calculated, and plotted as 3D isosurfaces. Optimized structures are checked against imaginary vibration frequencies to make sure that they are not saddle points in the energy landscape.

X-ray data collection and structure refinement

The data were collected on a Bruker APEX II Quazar three-circle diffractometer using monochromatized Mo-Kα X-radiation (λ = 0.71073 Å). Data integration and reduction were carried out using SAINT.[31] Absorption correction was performed using a multi-scan method implemented in SADABS.[32] Space groups were determined using XPREP implemented in APEX2.[33] The structure was solved using the direct methods procedure in SHELXS-97[34] and then refined by full-matrix least-squares refinements on F^2 using SHELXL-97. All non-hydrogen atoms were refined anisotropically using all reflections with $I > 2\sigma(I)$. Aromatic C-bound H atoms were positioned geometrically and refined using a riding mode. The hydroxyl atom H1 on oxygen O1 was correctly located using AFIX 147 instructions in SHELXL-97 and constrained to refine on its parent O atoms with $U_{iso}(H) = 1.5U_{eq}(O)$. Crystallographic data and refinement details of the data collection for compound **3** are given in Table S1 (ESI†). The molecular drawings were generated using the Mercury program.[35]

Materials

Optical spectra in the UV-visible region were recorded on a Shimadzu 2001 UV spectrophotometer using a 1 cm path length cuvette at room temperature. Mass spectra were recorded on a MALDI (matrix assisted laser desorption ionization) BRUKER Microflex LT using 2,5-dihydroxybenzoic acid as the matrix. NMR spectra were recorded in $CDCl_3$ solutions on a Varian 500 MHz spectrometer. IR spectra were recorded between 4000 and 600 cm^{-1} using a Perkin Elmer Spectrum 100 FT-IR spectrometer with an attenuated total reflection (ATR) accessory featuring a zinc selenide (ZnSe) crystal.

Synthesis

Methods. Phthalonitrile **4** and phthalocyanine **2**[36] were prepared following reported procedures. All reaction solvents were dried and purified as described by Perrin and Armarego.[37]

Preparation of phthalonitrile 3. 4,5-Dichlorophthalonitrile (4 g, 20 mmol) was dissolved in DMF (50 mL). 1-Hexanethiol (2.8 mL, 20 mmol), 6-mercapto-1-hexanol (2.7 mL, 20 mmol) and K_2CO_3 (22,08 g, 160 mmol) were successively added.

The mixture was stirred vigorously for 48 h then poured into water. The mixture was filtered. The residue was purified by column chromatography using first dichloromethane as the eluent, then dichloromethane/ethanol (100/1). The fraction containing the desired phthalonitrile **3** was chromatographed on a second silica gel column using a hexane/ethyl acetate mixture as the eluent. Yield 18% (1.40 g). $C_{20}H_{28}N_2OS_2$, M_W 376.58. White solid. m.p:89–91 °C. FT-IR ν_{max} (cm^{-1}) 3533, 2927, 2857, 2228, 1563, 1459, 1395, 1347, 1285, 1227, 1119, 1049, 1001, 933, 752, 689. HRMS *m*/*z*: 399.153 $[M + Na]^+$. ^1H NMR (500 MHz, $CDCl_3$) ppm: 7.42 (2H, s, ArCH), 3.67–3.65 (3H, m, CH_2O, OH), 3.04–3.00 (4H, q, CH_2–S), 1.79–1.33 (16H, m, CH_2), 0.92–0.90 (3H, t, CH_3). ^{13}C NMR (125 MHz, $CDCl_3$) ppm: 144.28, 144.03 (ArC–S), 128.12, 128.07 (ArCH), 115.66, 115.65 (CN), 111.04–110.96 (ArC–C), 62.65 (CH_2–O), 32.69, 32.57, 32.40, 31.20, 28.63, 28.62, 28.53, 27.98, 22.43 (CH_2), 25.27, 25.25 (CH_2S), 13.95 (CH_3). Anal. calc. for $C_{20}H_{28}N_2OS_2$ (376.57): C: 63.79; H: 7.49; N: 7.44; found: C: 63.89; H: 7.40; N: 7.43.

Preparation of phthalocyanine 1. To a mixture of phthalonitrile **3** (200 mg, 0.53 mmol) and phthalonitrile **4** (1.5 g, 4.16 mmol) in *n*-pentanol (4 mL) were added DBU (0.4 mL) and anhydrous zinc acetate (580 mg, 3.16 mmol). The reaction mixture was refluxed at 140 °C for 6 h and then the green product was poured into a water/ethanol mixture and filtered. The residue was purified using column chromatography using first dichloromethane, and then the polarity of the eluent was gradually increased up to that of dichloromethane/ethanol (20/1). **1** was fully purified using preparative silica thin layer chromatography using dichloromethane/ethanol (200/1). Yield 13% (110 mg). $C_{80}H_{112}N_8OS_8Zn$, M_W 1523.73. Deep green wax. FT-IR ν_{max} (cm^{-1}) 2954, 2924, 2854, 2572, 1592, 1483, 1457, 1404, 1369, 1335, 1281, 1260, 1085, 1066, 943, 897, 778, 741, 698. MALDI-TOF-MS (matrix DHB): *m*/*z* 1524.514 $[M + H]^+$. UV-Vis ($CHCl_3$) λ_{max} ($\log \varepsilon$) 370 (4.93), 710 (5.41).

Preparation of phthalocyanine–biotine conjugate 5. Biotine (146 mg, 0.6 mmol), *N*,*N*′-dimethylaminopyridine (1 equiv., 73 mg) and dicyclohexylcarbodiimide (1 equiv., 124 mg) were stirred two hours in DMF (2 mL), then phthalocyanine **1** (45 mg, 0.3 mmol) was added. Stirring of the reaction mixture at room temperature was continued overnight. After TLC control of the completion of the reaction, water was added to the reaction mixture which was filtered and thoroughly washed with a water/ethanol mixture (1/1). Phthalocyanine–biotine conjugate **5** was purified using preparative silica gel thin layer chromatography, eluent dichloromethane/ethanol (10/1). Yield 79% (41 mg). $C_{90}H_{126}N_{10}O_3S_9Zn$, M_W 1749.99. Deep green wax. MALDI-TOF-MS (matrix DHB): *m*/*z* 1751.18 $[M + H]^+$ and 1773.02 $[M + Na]^+$. UV-Vis ($CHCl_3$) λ_{max} ($\log \varepsilon$) 365 (3.51), 700 (3.88).

Acknowledgements

The Scientific and Technological Research Council of Turkey (TUBITAK) is gratefully acknowledged (project 112T670 coupled to the COST Action CM1105).

References

1 S. Z. Topal, Ü. İşci, U. Kumru, D. Atilla, A. G. Gürek, C. Hirel, M. Durmuş, J.-B. Tommasino, D. Luneau, S. Berber, F. Dumoulin and V. Ahsen, *Dalton Trans.*, 2014, **43**, 6897.
2 T. Nyokong, *Coord. Chem. Rev.*, 2007, **251**, 1707.
3 Y. Arslanoğlu, A. M. Sevim, E. Hamuryudan and A. Gül, *Dyes Pigm.*, 2005, **68**, 129.
4 D. Topkaya, F. Dumoulin, V. Ahsen and Ü. İşci, *Dalton Trans.*, 2014, **43**, 2032.
5 N. Kobayashi, H. Ogata, N. Nonaka and E. A. Luk'yanets, *Chem. – Eur. J.*, 2003, **9**, 5123.
6 D. Aydın Tekdaş, R. Garifullin, B. Şentürk, Y. Zorlu, U. Gundogdu, E. Atalar, A. B. Tekinay, A. A. Chernonosov, Y. Yerli, F. Dumoulin, M. O. Guler, V. Ahsen and A. G. Gürek, *Photochem. Photobiol.*, 2014, **90**, 1376.
7 S. Tuncel, A. Trivella, D. Atilla, K. Bennis, H. Savoie, F. Albrieux, L. Delort, H. Billard, V. Dubois, V. Ahsen, F. Caldefie-Chézet, C. Richard, R. W. Boyle, S. Ducki and F. Dumoulin, *Mol. Pharmaceutics*, 2013, **10**, 3706.
8 W. Duan, K. Smith, H. Savoie, J. Greenman and R. W. Boyle, *Org. Biomol. Chem.*, 2005, **3**, 2384.
9 D. Lafont, Y. Zorlu, H. Savoie, F. Albrieux, V. Ahsen, R. W. Boyle and F. Dumoulin, *Photodiagn. Photodyn. Ther.*, 2013, **10**, 252.
10 I. R. Vlahov and C. P. Leamon, *Bioconjugate Chem.*, 2012, **23**, 1357.
11 N. B. McKeown, *J. Mater. Chem.*, 2000, **10**, 1979.
12 F. Giuntini, F. Dumoulin, R. Daly, V. Ahsen, E. M. Scanlan, A. Lavado, J. W. Aylott, G. Rosser, A. Beeby and R. W. Boyle, *Nanoscale*, 2012, **4**, 2034.
13 S. Alpugan, Ü. İşci, F. Albrieux, C. Hirel, A. G. Gürek, Y. Bretonnière, V. Ahsen and F. Dumoulin, *Chem. Commun.*, 2014, **50**, 7466.
14 M. Kandaz, A. T. Bilgicli and A. Altindal, *Synth. Met.*, 2010, **160**, 52.
15 Y. Zorlu, D. Topkaya Taşkıran, D. K. Tarakçı, U. Kumru, S. Alpugan, Ü. İşci, F. Dumoulin and V. Ahsen, *J. Chem. Crystallogr.*, 2014, **44**, 337.
16 V. N. Nemykin, S. V. Dudkin, F. Dumoulin, C. Hirel, A. G. Gürek and V. Ahsen, *ARKIVOC*, 2014, **i**, 142.
17 A. Wang, L. Long and C. Zhang, *Tetrahedron*, 2012, **68**, 2433.
18 J. Mack and N. Kobayashi, *Chem. Rev.*, 2011, **111**, 281.
19 G. de la Torre and T. Torres, *J. Porphyrins Phthalocyanines*, 2002, **6**, 274.
20 R. Jones and O. Gunnarsson, *Rev. Mod. Phys.*, 1989, **61**, 689.
21 M.-R. Ke, S.-L. Yeung, D. K. P. Ng, W.-P. Fong and P.-C. Lo, *J. Med. Chem.*, 2013, **56**, 8475.
22 S. Wang, J. Wang and J.-Y. Chen, *J. Mater. Chem. B*, 2014, **2**, 1594.
23 J. Kim, C.-H. Tung and Y. Choi, *Chem. Commun.*, 2014, **50**, 10600.
24 D. Jung, S. Maiti, J. H. Lee, J. H. Lee and J. S. Kim, *Chem. Commun.*, 2014, **50**, 3044.
25 J. Garcia, S. Barluenga, K. Gorska, F. Sasse and N. Winssinger, *Bioorg. Med. Chem.*, 2012, **20**, 672.

26 I. G. Meerovich, V. V. Jerdeva, V. M. Derkacheva, G. A. Meerovich, E. A. Lukyanets, E. A. Kogan and A. P. Savitsky, *J. Photochem. Photobiol., B*, 2005, **80**, 57.
27 J. M. Soler, E. Artacho, J. D. Gale, A. García, J. Junquera, P. Ordejón and D. Sánchez-Portal, *J. Phys.: Condens. Matter*, 2002, **14**, 2745.
28 N. Troullier and J. L. Martins, *Phys. Rev. B: Condens. Matter Mater. Phys.*, 1991, **43**, 1993.
29 L. Kleinman and D. M. Bylander, *Phys. Rev. Lett.*, 1982, **48**, 1425.
30 J. P. Perdew, K. Burke and M. Ernzerhof, *Phys. Rev. Lett.*, 1996, **77**, 3865.
31 *SAINT V8.27B*, Bruker AXS Inc, Madison, Wisconsin, 2012.
32 *SADABS V2012/1*, Bruker AXS Inc, Madison, Wisconsin, 2012.
33 *APEX2 V2012.10-0*, Bruker AXS Inc., Madison, Wisconsin, USA, 2012.
34 G. M. Sheldrick, *Acta Crystallogr., Sect. A: Found. Crystallogr.*, 2008, **64**, 112–122.
35 C. F. Macrae, P. R. Edgington, P. McCabe, E. Pidcock, G. P. Shields, R. Taylor, M. Towler and J. van de Streek, *J. Appl. Crystallogr.*, 2006, **39**, 453.
36 A. G. Gürek and Ö. Bekaroglu, *J. Chem. Soc., Dalton Trans.*, 1994, 1419.
37 D. D. Perrin and W. L. F. Armarego, *Purification of Laboratory Chemicals*, Pergamon Press, Oxford, 2nd edn, 1989.